The potential impact of nuclear conflict on ocean acidification

Nicole S. Lovenduski[1,2], Cheryl S. Harrison[2,3], Holly Olivarez[2,4], Charles G. Bardeen[5,6], Owen B. Toon[1,6], Joshua Coupe[7], Alan Robock[7], Tyler Rohr[8], Samantha Stevenson[9]

[1]Department of Atmospheric and Oceanic Sciences, University of Colorado, Boulder, CO, USA
[2]Institute of Arctic and Alpine Research, University of Colorado, Boulder, CO, USA
[3]University of Texas Rio Grande Valley, Port Isabel, TX, USA
[4]Environmental Studies Program, University of Colorado, Boulder, CO, USA
[5]Atmospheric Chemistry Observations and Modeling Laboratory, National Center for Atmospheric Research, Boulder, CO, USA
[6]Laboratory for Atmospheric and Space Physics, University of Colorado, Boulder, CO, USA
[7]Department of Environmental Sciences, Rutgers University, New Brunswick, NJ, USA
[8]Water Power Technologies Office, Department of Energy, Washington, DC, USA
[9]Bren School of Environmental Science and Management, University of California, Santa Barbara, CA, USA

Key Points:

- Nuclear conflict has the potential to increase surface ocean pH and decrease aragonite saturation state
- The decrease in saturation state would exacerbate shell dissolution from anthropogenic ocean acidification
- A regional nuclear conflict may have far-reaching effects on global ocean carbonate chemistry

Corresponding author: Nicole S. Lovenduski, `nicole.lovenduski@colorado.edu`

Abstract

We demonstrate that the global cooling resulting from a range of nuclear conflict scenarios would temporarily increase the pH in the surface ocean by up to 0.06 units over a 5-year period, briefly alleviating the decline in pH associated with ocean acidification. Conversely, the global cooling dissolves atmospheric carbon into the upper ocean, driving a 0.1 to 0.3 unit decrease in the aragonite saturation state (Ω_{arag}) that persists for ~10 years. The peak anomaly in pH occurs 2 years post-conflict, while the Ω_{arag} anomaly peaks 4-5 years post-conflict. The decrease in Ω_{arag} would exacerbate a primary threat of ocean acidification: the inability of marine calcifying organisms to maintain their shells/skeletons in a corrosive environment. Our results are based on sensitivity simulations conducted with a state-of-the-art Earth system model integrated under various black carbon (soot) external forcings. Our findings suggest that regional nuclear conflict may have ramifications for global ocean acidification.

1 Introduction

Nuclear warfare could have devastating impacts on millions of people, yet it has been suggested that regional or global nuclear conflict may be possible in the future [*Toon et al.*, 2019]. In addition to the calamitous impacts of nuclear conflict on a local level, research conducted with a range of climate models finds a global cooling in response to various conflict scenarios [*Turco et al.*, 1983; *Malone et al.*, 1985; *Robock et al.*, 2007; *Mills et al.*, 2014; *Pausata et al.*, 2016; *Coupe et al.*, 2019]. This global cooling is driven by fires started by the nuclear weapons. These fires inject smoke into the upper troposphere, where rapid lofting can spread the sunlight-absorbing soot particles into the stratosphere [*Turco et al.*, 1983]. Recent research implies that even a small nuclear conflict may have impacts on the global climate system, affecting the state and circulation of the atmosphere [*Robock et al.*, 2007], increasing the sea ice extent in both hemispheres [*Mills et al.*, 2014], and reducing plant productivity and crop yields in regions far from the conflict location [*Özdoğan et al.*, 2013; *Xia and Robock*, 2013; *Toon et al.*, 2019].

While less studied, the potential impacts of nuclear conflict on the ocean are many. Numerous physical, chemical, and biological processes in the ocean are temperature-dependent, and sunlight is a critical ingredient for photosynthesizing phytoplankton at the base of the marine food web. Using a climate model with an interactive ocean, *Mills et al.* [2014] evaluated the ocean physical response to a potential India/Pakistan nuclear war that lofts 5 Tg of black carbon particles into the stratosphere; they find an 0.8°C decrease in globally-averaged sea surface temperature, with smaller temperature reductions at depth. Recently *Toon et al.* [2019] used an Earth system model that includes a representation for phytoplankton to evaluate the ocean biological response to nuclear conflict; they report a 5-15% decrease in phytoplankton productivity under a range of conflict scenarios. Such findings prompt further investigation into how nuclear conflict and the resulting global cooling may alter the chemical state of the ocean. Perturbations in the ocean's carbonate chemistry are of particular interest, owing to their importance for ocean acidification.

Ocean acidification is an ongoing, large scale environmental problem driven by fossil fuel emissions of carbon dioxide (CO_2). Cumulatively since the pre-industrial era, the ocean has absorbed 41% of the carbon emitted by human industrial activities [*McKinley et al.*, 2017]. While this ocean absorption of carbon has partially mitigated anthropogenic global warming, it has fundamentally altered the carbonate chemistry of the ocean, increasing the concentration of hydrogen ions ($[H^+]$), while decreasing the concentration of carbonate ions ($[CO_3^{2-}]$). Observations collected at time series sites across the global ocean find statistically significant reductions in the potential hydrogen (pH = $-\log([H^+])$) and the saturation state of the calcium carbonate mineral aragonite (Ω_{arag}, which is proportional to $[CO_3^{2-}]$) over the past few decades [*Bates et al.*, 2014]. These changes are

a direct consequence of the ocean absorption of anthropogenic carbon; carbonate chemistry dictates that the excess carbon will react with water and CO_3^{2-} to decrease ocean pH and Ω_{arag} [*Feely et al.*, 2004]. Both of these changes may have negative consequences for marine organisms, in particular for those that precipitate calcium carbonate shells (e.g., coccolithophores, pteropods, foraminifera, corals, molluscs, echinoderms), as the precipitation is hindered by low pH, and because decreases in Ω_{arag} favor shell dissolution [*Doney et al.*, 2009].

To date, there have been no studies of the effects of nuclear conflict on ocean acidification, though past modeling studies on the ocean's response to volcanic forcing and to proposed geoengineering schemes have intimated that ocean carbonate chemistry is highly sensitive to these types of external forcings. Using a fully-coupled carbon-climate model, *Frölicher et al.* [2011] find that volcanic-induced cooling following the 1991 Mt. Pinatubo eruption led to immediate increases in the flux of carbon from atmosphere to ocean and consequently, increases in the total dissolved inorganic carbon (DIC) concentration in the surface ocean. *Eddebbar et al.* [2019] demonstrate that air-to-sea CO_2 fluxes are significantly enhanced following the eruptions of Agung, El Chichón, and Pinatubo in a large ensemble of simulations with an Earth system model. *Matthews et al.* [2009] conduct solar radiation management climate engineering simulations with an intermediate complexity model of the coupled climate-carbon system; they find changes in ocean pH and Ω_{arag} as a result of the anomalous cooling. Similarly, *Lauvset et al.* [2017] indicate that radiation management geoengineering leads to changes in North Atlantic pH in a fully coupled Earth system model, but do not explore changes in Ω_{arag}. While these studies are suggestive of the carbonate chemistry response to nuclear conflict, the external forcing perturbations are of a different magnitude and duration than those imposed by nuclear conflict. Further, it is difficult to mechanistically understand the ocean carbonate chemistry response to such external forcing perturbations in fully coupled models, where the terrestrial response to forcing additionally influences the atmospheric CO_2 concentration.

Here, we use a state-of-the art Earth system model to simulate the ocean carbonate chemistry response to a range of nuclear conflict scenarios. We decouple the ocean carbon cycle from that of the terrestrial carbon cycle via a direct prescription of the atmospheric CO_2 boundary condition used for air-sea CO_2 flux, i.e., changes in the terrestrial biosphere have no influence on the atmospheric CO_2 that the ocean sees. As we will demonstrate, we find large perturbations in ocean pH and Ω_{arag} as a result of nuclear conflict. These perturbations have relatively long duration (order 10 years), and are driven by decreases in temperature and subsequent increases in the ocean carbon inventory.

2 Methods

We analyze output generated by the Community Earth System Model (CESM) version 1.3, a state-of-the-art coupled climate model consisting of atmosphere, ocean, land, and sea ice components [*Hurrell et al.*, 2013]. The atmosphere component of CESM in our simulations is the Whole Atmosphere Community Climate Model [WACCM; *Marsh et al.*, 2013] with nominal 2° resolution, 66 vertical levels, and a model top at ∼145 km; it uses the Rapid Radiative Transfer Model for GCMs [RRTMG; *Iacono et al.*, 2000] for the radiative transfer. The Community Aerosol and Radiation Model for Atmospheres [CARMA; *Bardeen et al.*, 2008] is coupled with WACCM to simulate the injection, lofting, advection, and removal of soot aerosols in the troposphere and stratosphere, and their subsequent impact on climate [*Coupe et al.*, 2019; *Toon et al.*, 2019]. The ocean component of CESM is the Parallel Ocean Program (POP) version 2 [*Danabasoglu et al.*, 2012] with nominal 1° resolution and 60 vertical levels. The biogeochemical ocean component of CESM is the Biogeochemical Elemental Cycling (BEC) model that represents the lower trophic levels of the marine ecosystem, full carbonate system thermodynamics, air-sea

127 CO_2 fluxes, and a dynamic iron cycle [*Moore et al.*, 2004; *Doney et al.*, 2006; *Moore and*
128 *Braucher*, 2008; *Moore et al.*, 2013; *Long et al.*, 2013; *Lindsay et al.*, 2014].

129   The ocean in the coupled CESM simulation is initialized from rest with World Ocean
130 Circulation (WOCE) temperature and salinity [*Gouretski and Koltermann*, 2004]. Bio-
131 geochemical tracers are initialized to observationally based climatologies where possi-
132 ble [*Lauvset et al.*, 2016]; where these were not available (such as dissolved iron and phy-
133 toplankton biomass), the model is initialized with fields interpolated from an existing
134 CESM simulation. The new, fully coupled simulation was spun up for four years to an
135 approximate steady state with a constant atmospheric CO_2 mixing ratio of 370 ppm, rep-
136 resentative of the mixing ratio in the year 2000. Due to the relatively short spin-up pe-
137 riod, the globally integrated air-sea CO_2 flux is not in steady state (drifting at a rate of
138 0.14 Pg C yr^{-2}) when the perturbation forcing is applied. We therefore present our re-
139 sults as anomalies from the drifting control integrations.

140   Three control simulations of 20-year duration are generated using round-off level
141 differences in atmospheric initial conditions. As each of these control simulations has dif-
142 ferent phasing of internal variability (e.g., El Niño - Southern Oscillation, or ENSO), we
143 use the standard deviation across this ensemble to identify statistically significant per-
144 turbations due to nuclear conflict.

145   We report on the anomalies generated from four simulations of nuclear conflict with
146 varying amounts of soot injection: three India/Pakistan conflict scenarios that inject 5,
147 27, and 47 Tg of soot, respectively, and one US/Russia conflict scenario that injects 150
148 Tg of soot. The initial soot injection amounts are generated from plausible scenarios for
149 nuclear conflict following advice from a number of military and policy experts; the reader
150 is referred to *Toon et al.* [2019] for further details on scenario development. In each case,
151 we prescribe that the conflict begins on May 15 of the 5th year of the first control sim-
152 ulation and we integrate the model for a 15-year period following the injection. We as-
153 sume that the smoke generated by mass fires from nuclear conflict is injected into the
154 upper troposphere above the target sites (in the US/Russia case, smoke is spread evenly
155 over the two nations), as in *Toon et al.* [2019]. WACCM lofts much of this smoke higher
156 into the stratosphere via solar heating of black carbon aerosols in the smoke, where the
157 black carbon aerosols persist for about a decade. The resulting annual-mean, post-conflict
158 (May to the following April) anomalies in aerosol optical depth are shown in Figure 1a.
159 These optical depth changes result in a 10-40% reduction in incoming solar energy [*Toon*
160 *et al.*, 2019]. While we discuss the anomalies generated from all four of these conflict sim-
161 ulations, we describe two in greater detail throughout this manuscript: the US/Russia
162 case, as it is the largest climate perturbation overall, and the India/Pakistan 47 Tg case,
163 as it is the largest climate perturbation generated by a regional nuclear conflict.

164   Ocean biogeochemistry in the version of CESM used for our simulations has been
165 extensively validated in the literature [*Long et al.*, 2013; *Moore et al.*, 2013; *Lindsay et al.*,
166 2014; *Lovenduski et al.*, 2015; *Long et al.*, 2016; *Lovenduski et al.*, 2016; *McKinley et al.*,
167 2016; *Krumhardt et al.*, 2017; *Freeman et al.*, 2018; *Harrison et al.*, 2018; *Brady et al.*,
168 2019; *Negrete-García et al.*, 2019]. Of particular note for our study, the simulated sur-
169 face ocean carbonate ion concentration from a long, preindustrial control simulation of
170 CESM compares favorably with reconstructed observations, albeit with lower interan-
171 nual variance than has been measured at subtropical time-series sites [*Lovenduski et al.*,
172 2015]. In Figure S1, we illustrate the comparison between observationally based estimates
173 of surface ocean pH and Ω_{arag} [from GLODAPv2; *Lauvset et al.*, 2016] and the CESM
174 control ensemble mean. In this comparison, we note that the observational estimates have
175 been extensively interpolated and are intended to represent year 2002 carbonate chem-
176 istry parameters, whereas CESM has been integrated under an atmospheric CO_2 mix-
177 ing ratio that corresponds to year 2000 forcing. We find high correspondence between
178 the spatial patterns of modeled and observed pH and Ω_{arag}, giving us confidence that
179 CESM is capable of representing the mean state of these two variables.

3 Results

Globally averaged surface ocean pH increases in response to each of the nuclear conflicts, where the magnitude of the pH anomaly scales with the amount of soot injected (Figure 1b). In each case, the pH anomaly exceeds the interannual standard deviation of pH in the control ensemble mean (gray shading in Figure 1b). We observe the largest increases in surface ocean pH in response to the US/Russia 150 Tg case; here the globally averaged surface ocean pH anomaly exceeds 0.05, corresponding to a ∼10% decrease in the global-mean hydrogen ion concentration. Under each scenario, the pH anomaly peaks 2-4 years after the conflict and persists for ∼10 years. With the exception of the high latitude oceans, the pH increase following the nuclear conflict is pervasive across the surface ocean (Figures 2a-c). In the 47 Tg India/Pakistan scenario, we observe local pH anomalies exceeding 0.06 units on average in years 2-5 post-conflict (Figure 2c); the anomalies are largest in the North Atlantic, North Pacific, and Equatorial Pacific. These large, abrupt changes in surface ocean pH may have important consequences for calcifying organisms, as shell precipitation can be affected by the ambient hydrogen ion concentration in seawater [*Kroeker et al.*, 2013]. Since the beginning of the industrial revolution, global ocean pH has dropped by an estimated 0.1 units [*Ciais and Sabine*, 2013]. The anomalies in pH generated by our simulations exceed 50% of this historical change, and occur over a much shorter time period. Whether and how organisms respond to the initial and rapid alleviation of low pH, followed by an immediate return to the current pH state in the global ocean is as yet unknown [see, e.g., *Haigh et al.*, 2015].

In contrast to our results for pH, we observe decreases in surface ocean Ω_{arag} following nuclear conflict (Figure 1c), which should tend to inhibit the maintenance of shells and skeletons in calcified organisms. While minimal changes in Ω_{arag} are simulated for the 5 Tg India/Pakistan case, the other three cases produce large decreases in saturation state, on the order of 0.1 to 0.3 units (Figure 1c). In each of these three cases, the anomalies exceed the interannual standard deviation of Ω_{arag} in the control ensemble mean (gray shading in Figure 1c). The peak response in these three cases occurs 3-5 years post-conflict, a year or so later than the pH response. While for pH the globally averaged anomaly is negligibly small 10 years post-conflict, anomalies in globally averaged Ω_{arag} persist beyond our 15-year simulation timeframe for all conflict scenarios. The decreases in aragonite saturation state span the tropics and subtropics, with the exception of the central and eastern Equatorial Pacific region (Figures 2d-f). Local decreases in saturation state exceed 0.5 units in the western North Atlantic and western North Pacific under the 47 Tg India/Pakistan scenario (Figure 2f). Importantly, the simulated decreases in saturation state are highly pronounced in regions that host diverse coral reef ecosystems (for instance, the western and southwestern Pacific and the Caribbean), and like pH, the changes in saturation state occur fairly rapidly. Projections from climate models suggest that coral reef ecosystems across the world will experience aragonite saturation state declines from their preindustrial value of 3.5 to 3.0 by the end of the century [*Ricke et al.*, 2013]; alarmingly, our simulations project similar Ω_{arag} declines over a 3-5 year period, which then persist for years after the initial forcing dissipates.

The opposite-signed anomalies in pH and Ω_{arag} induced by nuclear conflict seem puzzling at first, as for 'typical' anthropogenic ocean acidification scenarios, both of these variables simultaneously decrease. Why would nuclear conflict cause opposing responses in pH and saturation state? To understand these opposing responses, we need to consider the carbonate chemistry system in seawater and its sensitivity to changing temperature. Gaseous CO_2 reacts with seawater to form carbonic acid (H_2CO_3), which then dissociates to form H^+ and bicarbonate (HCO_3^-). The hydrogen ion then reacts with CO_3^{2-} to form additional HCO_3^-,

$$CO_2 + H_2O \rightleftharpoons H_2CO_3 \tag{1}$$

$$H_2CO_3 \rightleftharpoons H^+ + HCO_3^- \tag{2}$$

$$H^+ + CO_3^{2-} \rightleftharpoons HCO_3^-. \tag{3}$$

$$\tag{4}$$

The equilibrium constants for these reactions [typically expressed as K_0, K_1, and K_2, respectively; *Sarmiento and Gruber*, 2006] are sensitive to changes in temperature, e.g., the cooling induced by nuclear conflict. We need to also consider the dissolution reaction for mineral calcium carbonate ($CaCO_3$) in seawater,

$$CaCO_3(s) \rightleftharpoons Ca_{sat}^{2+} + CO_{3,sat}^{2-}, \tag{5}$$

where $[Ca^{2+}]_{sat}$ and $[CO_3^{2-}]_{sat}$ are the concentrations of dissolved calcium and carbonate in equilibrium with mineral $CaCO_3$, and the solubility product (K_{sp}) for this reaction is also sensitive to temperature [*Sarmiento and Gruber*, 2006]. Further, the saturation state for a calcium carbonate mineral in seawater (here: aragonite), can be expressed as

$$\Omega_{arag} = \frac{[Ca^{2+}][CO_3^{2-}]}{K_{sp}}, \tag{6}$$

where both $[CO_3^{2-}]$ and K_{sp} are affected by changes in temperature [Ca^{2+} is highly abundant in seawater and thus changes in temperature do not affect its concentration enough to matter for $CaCO_3$ dissolution; *Sarmiento and Gruber*, 2006; *Emerson and Hedges*, 2008]. Thus, we can decompose the anomalies in pH and Ω_{arag} into the component driven by temperature-induced changes in the carbonate chemistry equilibrium constants (K_0, K_1, K_2, K_{sp}) and the component driven by all other changes to the carbonate chemistry system, such as changes in the dissolved inorganic carbon (DIC) concentration, the alkalinity, or the salinity. We approximate the temperature sensitivity of the equilibrium constants using a program developed for CO_2 system calculations [CO2SYS; *van Heuven et al.*, 2011] via finite difference approximation. The component driven by all other changes to the carbonate system is computed as the residual of the other two terms.

The pH response to nuclear conflict is the sum of two opposing drivers: an increase in pH driven by a decrease in sea surface temperature that alters the carbonate chemistry equilibrium constants, and a decrease in pH driven by an increase in the DIC concentration of the upper ocean. Figure 1b illustrates the temporal evolution of the components of the global pH anomalies from the India/Pakistan 47 Tg simulation driven by changes in the equilibrium constants versus all other changes in the carbonate chemistry system. The equilibrium constant-driven pH anomaly is positive, peaking 2-3 years after the conflict, whereas the "other" component of the pH anomaly is negative, peaking 3-5 years after the conflict. The resulting total pH anomaly is positive, indicating that it is more strongly influenced by changes in the equilibrium constants than other changes. In the India/Pakistan 47 Tg case, globally averaged temperature reaches a minimum 2-3 years post-conflict; the model initially produces 3.5-4°C anomalies at the surface that re-warm toward pre-conflict values for the duration of the simulation (Figure 3a). In contrast, surface ocean salinity-normalized DIC anomalies peak 3-5 years post-conflict (Figure 3b), mainly as a result of the enhanced solubility of CO_2 in colder seawater. While decreasing biological export production also contributes to increased DIC in the surface ocean, this signal is small relative to the change driven by enhanced air-to-sea CO_2 flux (e.g., Figure S2). The delay in DIC relative to temperature anomalies is a result of the long (order months to years) timescale for CO_2 to fully equilibrate with the surface mixed layer [*Emerson and Hedges*, 2008]. The cold, high DIC surface anomalies slowly propagate into the global ocean thermocline; we observe 1°C and 10 mmol m^{-3} anomalies in temperature and DIC, respectively at a depth of 300 m that persist beyond the length

of our simulation (Figure 3). As there are no significant anomalies in global-mean alkalinity or salinity post-conflict (not shown), we conclude that the DIC perturbation drives the "other" component of the pH anomalies. We find similar behavior for these components in the other conflict scenarios (not shown).

The negative Ω_{arag} anomalies post-conflict are driven by a combination of lower temperatures and higher DIC concentrations. Colder surface temperatures tend to increase K_{sp}, while higher surface DIC concentrations tend to decrease $[CO_3^{2-}]$, resulting in lower Ω_{arag} values post-conflict. Figure 1c illustrates that the DIC (other) component dominates the total Ω_{arag} anomaly for the India/Pakistan 47 Tg simulation. As for pH, the equilibrium constant component peaks earlier than the other component; this is due to the timing of the temperature and DIC perturbations (Figure 3).

The spatial patterns of the post-conflict surface pH and Ω_{arag} anomalies in the India/Pakistan 47 Tg scenario (Figure 2c,f) result from perturbations in local surface ocean temperature and DIC (Figure S3). Negative temperature anomalies and positive DIC anomalies are pervasive in the tropics and extratropics, with the exception of the eastern Equatorial Pacific, where a large and long-lasting El Niño-like event develops following the conflict [*Coupe, et al.,* manuscript in review]. This strong reduction in the equatorial trade winds greatly weakens upwelling in the cold tongue region, producing near-zero surface temperature anomalies and a reduction in vertical DIC supply here (Figure S3). In the Southern Ocean, temperature and DIC are not much affected by the nuclear conflict, likely a result of enhanced upwelling of warm water from the subsurface [*Harrison, et al.,* manuscript in preparation]. Taken together, the aforementioned changes in temperature and DIC lead to increases in pH and decreases in Ω_{arag} over most of the ocean surface (Figure S4).

The changes in surface ocean pH that we simulate for nuclear conflict resemble the simulated response of pH to volcanic eruptions, but are an order of magnitude larger. Figure S5 illustrates the anomaly in surface ocean pH in the first year following the eruptions of Agung, El Chichón, and Mt. Pinatubo, as estimated by the CESM Large Ensemble [*Kay et al.,* 2015], which uses the same physical and biogeochemical ocean components as in our nuclear conflict simulations. The ensemble mean isolates the evolution of the Earth system under historical external forcing, including the aerosol loading following volcanic eruptions [*Eddebbar et al.,* 2019], and averages across the various representations of internal variability [*Deser et al.,* 2012]. (We note that ensembles are not necessary for the nuclear conflict scenarios, since the much larger magnitude of forcing provides a higher signal-to-noise ratio). The anomaly in the ensemble mean shown here thus cleanly captures the response of surface ocean pH to volcanic eruptions. Here we show the anomaly in preindustrial pH (pH anomalies in equilibrium with preindustrial atmospheric CO_2, which is computed simultaneously with contemporary pH at model run time), as the contemporary pH anomalies include also the response to increasing atmospheric CO_2 from one year to the next. The similarity in the spatial patterns of volcanically induced pH anomalies and those produced under nuclear conflict is striking (cf. Figures S5 and 2c), suggesting that volcanic forcing produces similar temperature, DIC and thus pH anomalies [including the El Niño-like response to volcanic forcing in the eastern Equatorial Pacific, described in *Eddebbar et al.,* 2019]. However, the eruption-driven pH anomaly is both smaller (an order of magnitude) and of shorter duration (∼2 years) than in the India/Pakistan 47 Tg simulation. Unfortunately, a similar analysis of volcanic Ω_{arag} anomalies in the CESM Large Ensemble was not possible as preindustrial $[CO_3^{2-}]$ was not saved to disk.

4 Conclusions and Discussion

We report on the surface ocean pH and Ω_{arag} anomalies generated from four simulations of nuclear conflict using the CESM with full ocean carbonate system thermo-

dynamics. Globally averaged surface ocean pH increases in response to each conflict, with the largest increases in the North Atlantic, North Pacific, and Equatorial Pacific Ocean. The pH anomalies persist for 10 years post-conflict, and are primarily driven by changes in the carbonate chemistry equilibrium constants as a result of decreases in sea surface temperature. In contrast, CESM simulates globally averaged decreases in surface ocean Ω_{arag} in response to nuclear conflict, with the largest decreases in the tropics and sub-tropics. The Ω_{arag} anomalies persist beyond the length of our 15-year simulations and are driven by a combination of changes in the carbonate chemistry equilibrium constants and the solubility-driven increases in DIC. We further demonstrate that the surface pH anomalies induced by nuclear conflict resemble those induced by volcanic eruptions in the same modeling system.

The simulated changes in global and regional pH and Ω_{arag} as a result of nuclear conflict are large and abrupt. In the most extreme forcing scenario (US/Russia 150 Tg), over a period of ∼5 years, global surface ocean pH increases by 0.06 units and Ω_{arag} decreases by 0.3 units. To put these numbers into perspective, this simulated rate of change of pH is 10 times larger than the rate of change we have observed over the past 2 decades as a result of ocean acidification [-0.0018 yr^{-1}; *Lauvset et al.*, 2015]. Worryingly, surface ocean Ω_{arag} decreases more than 6 times faster than has been observed in the open ocean over the past 3 decades [-0.0095 yr^{-1} at the Bermuda Atlantic Time-series; *Bates et al.*, 2014]. While the cooling associated with nuclear conflict rapidly and briefly alleviates the decline in pH associated with ocean acidification, the increase in solubility causes the ocean to absorb ∼11 Pg of excess carbon in a 10-year period, leading to a rapid drop in Ω_{arag}.

Whether and how calcifying organisms might respond to such rapid and opposing changes in pH and Ω_{arag} is as yet unknown. In order to measure organism response to ocean acidification, a majority of laboratory studies perform CO_2 bubbling perturbation experiments, which simultaneously decrease the pH and Ω_{arag} in the surrounding seawater solution [*Pörtner et al.*, 2014]. This simultaneous change in two carbonate chemistry parameters challenges our ability to isolate the organism response to changes in pH or changes in Ω_{arag} alone. A recent laboratory sensitivity study of marine bivalve larve used chemical manipulation experiments to decouple these two parameters; they found that larval shell development and growth were negatively impacted by decreasing Ω and unaffected by changes in pH [*Waldbusser et al.*, 2014]. If these sensitivities are sustained in other organisms, we might conclude that calcifying organisms would be severely affected by nuclear conflict.

Our findings shed light on the ocean biogeochemical response to other forms of extreme external forcing, such as volcanic eruptions [*Frölicher et al.*, 2011; *Eddebbar et al.*, 2019] and solar radiation management climate engineering [*Matthews et al.*, 2009; *Lauvset et al.*, 2017]. They may further inform the study and understanding of the role of ocean acidification in marine extinction following the Chicxulub impact event [*Henehan et al.*, 2019]. Importantly, our results suggest that even a regional nuclear conflict can have an impact on global ocean acidification, adding to the list of the many, far-reaching consequences of nuclear conflict for global society.

References

Bardeen, C. G., O. B. Toon, E. J. Jensen, D. R. Marsh, and V. L. Harvey (2008), Numerical simulations of the three-dimensional distribution of meteoric dust in the mesosphere and upper stratosphere, *J. Geophys. Res. Atm.*, *113*(D17), doi: 10.1029/2007JD009515.

Bates, N. R., Y. M. Astor, M. J. Church, K. Currie, J. E. Dore, M. Gonzalez-Davila, L. Lorenzoni, F. Muller-Karger, J. Olaffson, and J. M. Santana-Casiano (2014), A time-series view of changing ocean chemistry due to ocean uptake of anthropogenic CO_2 and ocean acidification, *Oceanography*, *27*(1), 126–141.

Brady, R. X., N. S. Lovenduski, M. A. Alexander, M. Jacox, and N. Gruber (2019), On the role of climate modes in modulating the air–sea CO_2 fluxes in eastern boundary upwelling systems, *Biogeosciences*, *16*(2), 329–346, doi:10.5194/bg-16-329-2019.

Ciais, P., and C. Sabine (2013), Chapter 6: Carbon and Other Biogeochemical Cycles, in *Climate Change 2013: The Physical Science Basis. Contribution of Working Group I to the Fifth Assessment Report of the Intergovernmental Panel on Climate Change*, edited by T. F. Stocker, D. Qin, G.-K. Plattner, M. M. B. Tignor, S. K. Allen, J. Boschung, A. Nauels, Y. Xia, V. Bex, and P. M. Midgley, p. 1535 pp, Cambridge University Press, Cambridge, United Kingdom and New York, NY, USA.

Coupe, J., C. G. Bardeen, A. Robock, and O. B. Toon (2019), Nuclear winter responses to nuclear war between the United States and Russia in the Whole Atmosphere Community Climate Model Version 4 and the Goddard Institute for Space Studies ModelE, *J. Geophys. Res. Atm.*, *124*(15), 8522–8543, doi: 10.1029/2019JD030509.

Danabasoglu, G., S. C. Bates, B. P. Briegleb, S. R. Jayne, M. Jochum, W. G. Large, S. Peacock, and S. G. Yeager (2012), The CCSM4 Ocean Component, *J. Climate*, *25*(5), 1361–1389.

Deser, C., A. Phillips, V. Bourdette, and H. Teng (2012), Uncertainty in climate change projections: the role of internal variability, *Clim. Dynam.*, *38*(3-4), 527–546, doi:10.1007/s00382-010-0977-x.

Doney, S. C., K. Lindsay, I. Fung, and J. John (2006), Natural Variability in a Stable, 1000-Yr Global Coupled Climate–Carbon Cycle Simulation, *J. Climate*, *19*(13), 3033–3054.

Doney, S. C., V. J. Fabry, R. A. Feely, and J. A. Kleypas (2009), Ocean Acidification: The other CO_2 Problem, *Annu. Rev. Mar. Sci.*, *1*(1), 169–192, doi: 10.1146/annurev.marine.010908.163834.

Eddebbar, Y. A., K. B. Rodgers, M. C. Long, A. C. Subramanian, S.-P. Xie, and R. F. Keeling (2019), El Niño–like physical and biogeochemical ocean response to tropical eruptions, *J. Climate*, *32*(9), 2627–2649, doi:10.1175/JCLI-D-18-0458.1.

Emerson, S. R., and J. I. Hedges (2008), *Chemical Oceanography and the Marine Carbon Cycle*, Cambridge University Press, Cambridge, United Kingdom.

Feely, R. A., C. L. Sabine, K. Lee, W. Berelson, J. Kleypas, V. J. Fabry, and F. J. Millero (2004), Impact of Anthropogenic CO_2 on the $CaCO_3$ System in the Oceans, *Science*, *305*(5682), 362–366, doi:10.1126/science.1097329.

Freeman, N. M., N. S. Lovenduski, D. R. Munro, K. M. Krumhardt, K. Lindsay, M. C. Long, and M. Maclennan (2018), The variable and changing Southern Ocean Silicate Front: Insights from the CESM Large Ensemble, *Global Biogeochem. Cycles*, *32*(5), 752–768, doi:10.1029/2017GB005816.

Frölicher, T. L., F. Joos, and C. C. Raible (2011), Sensitivity of atmospheric CO_2 and climate to explosive volcanic eruptions, *Biogeosciences*, *8*(8), 2317–2339, doi:10.5194/bg-8-2317-2011.

Gouretski, V. V., and K. P. Koltermann (2004), WOCE Global Hydrographic Climatology, *Tech. rep.*, Berichte des Bundesamtes für Seeschifffahrt und Hydrographie

Nr. 35/2004.

Haigh, R., D. Ianson, C. A. Holt, H. E. Neate, and A. M. Edwards (2015), Effects of ocean acidification on temperate coastal marine ecosystems and fisheries in the Northeast Pacific, *PLoS ONE*, *10*(2), e0117,533–.

Harrison, C. S., M. C. Long, N. S. Lovenduski, and J. K. Moore (2018), Mesoscale effects on carbon export: A global perspective, *Global Biogeochem. Cycles*, *32*(4), 680–703, doi:10.1002/2017GB005751.

Henehan, M. J., A. Ridgwell, E. Thomas, S. Zhang, L. Alegret, D. N. Schmidt, J. W. B. Rae, J. D. Witts, N. H. Landman, S. E. Greene, B. T. Huber, J. R. Super, N. J. Planavsky, and P. M. Hull (2019), Rapid ocean acidification and protracted Earth system recovery followed the end-Cretaceous Chicxulub impact, *Proc. Nat. Acad. Sci.*, *201905989*, doi:10.1073/pnas.1905989116.

Hurrell, J. W., M. M. Holland, P. R. Gent, S. Ghan, J. E. Kay, P. J. Kushner, J. F. Lamarque, W. G. Large, D. Lawrence, K. Lindsay, W. H. Lipscomb, M. C. Long, N. Mahowald, D. R. Marsh, R. B. Neale, P. Rasch, S. Vavrus, M. Vertenstein, D. Bader, W. D. Collins, J. J. Hack, J. Kiehl, and S. Marshall (2013), The Community Earth System Model: A Framework for Collaborative Research, *B. Am. Meteorol. Soc.*, *94*(9), 1339–1360, doi:10.1175/BAMS-D-12-00121.1.

Iacono, M. J., E. J. Mlawer, S. A. Clough, and J.-J. Morcrette (2000), Impact of an improved longwave radiation model, RRTM, on the energy budget and thermodynamic properties of the NCAR community climate model, CCM3, *J. Geophys. Res. Atm.*, *105*(D11), 14,873–14,890, doi:10.1029/2000JD900091.

Kay, J. E., C. Deser, A. Phillips, A. Mai, C. Hannay, G. Strand, J. M. Arblaster, S. C. Bates, G. Danabasoglu, J. Edwards, M. Holland, P. Kushner, J. F. Lamarque, D. Lawrence, K. Lindsay, A. Middleton, E. Munoz, R. Neale, K. Oleson, L. Polvani, and M. Vertenstein (2015), The Community Earth System Model (CESM) Large Ensemble project: A community resource for studying climate change in the presence of internal climate variability, *B. Am. Meteorol. Soc.*, *96*(8), 1333–1349, doi:10.1175/BAMS-D-13-00255.1.

Kroeker, K. J., R. L. Kordas, R. Crim, I. E. Hendriks, L. Ramajo, G. S. Singh, C. M. Duarte, and J.-P. Gattuso (2013), Impacts of ocean acidification on marine organisms: quantifying sensitivities and interaction with warming, *Glob. Change Biol.*, *19*(6), 1884–1896, doi:10.1111/gcb.12179.

Krumhardt, K. M., N. S. Lovenduski, M. C. Long, and K. Lindsay (2017), Avoidable impacts of ocean warming on marine primary production: Insights from the CESM ensembles, *Global Biogeochem. Cycles*, *31*(1), 114–133, doi: 10.1002/2016GB005528.

Lauvset, S. K., N. Gruber, P. Landschützer, A. Olsen, and J. Tjiputra (2015), Trends and drivers in global surface ocean pH over the past 3 decades, *Biogeosciences*, *12*(5), 1285–1298, doi:10.5194/bg-12-1285-2015.

Lauvset, S. K., R. M. Key, A. Olsen, S. van Heuven, A. Velo, X. Lin, C. Schirnick, A. Kozyr, T. Tanhua, M. Hoppema, S. Jutterström, R. Steinfeldt, E. Jeansson, M. Ishii, F. F. Perez, T. Suzuki, and S. Watelet (2016), A new global interior ocean mapped climatology: the 1° x 1° GLODAP version 2, *Earth Syst. Sci. Data*, *8*(2), 325–340, doi:10.5194/essd-8-325-2016.

Lauvset, S. K., J. Tjiputra, and H. Muri (2017), Climate engineering and the ocean: effects on biogeochemistry and primary production, *Biogeosciences*, *14*(24), 5675–5691, doi:10.5194/bg-14-5675-2017.

Lindsay, K., G. B. Bonan, S. C. Doney, F. M. Hoffman, D. M. Lawrence, M. C. Long, N. M. Mahowald, J. Keith Moore, J. T. Randerson, and P. E. Thornton (2014), Preindustrial-control and twentieth-century carbon cycle experiments with the Earth System Model CESM1(BGC), *J. Climate*, *27*(24), 8981–9005, doi:10.1175/JCLI-D-12-00565.1.

Long, M. C., K. Lindsay, S. Peacock, J. K. Moore, and S. C. Doney (2013), Twentieth-Century Oceanic Carbon Uptake and Storage in CESM1(BGC), *J. Climate*, *26*(18), 6775–6800, doi:10.1175/JCLI-D-12-00184.1.

Long, M. C., C. Deutsch, and T. Ito (2016), Finding forced trends in oceanic oxygen, *Global Biogeochem. Cycles*, *30*(2), 381–397, doi:10.1002/2015GB005310, 2015GB005310.

Lovenduski, N. S., M. C. Long, and K. Lindsay (2015), Natural variability in the surface ocean carbonate ion concentration, *Biogeosciences*, *12*(21), 6321–6335, doi:10.5194/bg-12-6321-2015.

Lovenduski, N. S., G. A. McKinley, A. R. Fay, K. Lindsay, and M. C. Long (2016), Partitioning uncertainty in ocean carbon uptake projections: Internal variability, emission scenario, and model structure, *Global Biogeochem. Cycles*, *30*(9), 1276–1287, doi:10.1002/2016GB005426, 2016GB005426.

Malone, R. C., L. H. Auer, G. A. Glatzmaier, W. M. C., and O. B. Toon (1985), Influence of solar heating and precipitation scavenging on the simulated lifetime of post—nuclear war smoke, *Science*, *230*(4723), 317, doi: 10.1126/science.230.4723.317.

Marsh, D. R., M. J. Mills, D. E. Kinnison, J.-F. Lamarque, N. Calvo, and L. M. Polvani (2013), Climate change from 1850 to 2005 simulated in CESM1(WACCM), *J. Climate*, *26*(19), 7372–7391, doi:10.1175/JCLI-D-12-00558.1.

Matthews, H. D., L. Cao, and K. Caldeira (2009), Sensitivity of ocean acidification to geoengineered climate stabilization, *Geophys. Res. Lett.*, *36*(10), doi: 10.1029/2009GL037488.

McKinley, G. A., D. J. Pilcher, A. R. Fay, K. Lindsay, M. C. Long, and N. S. Lovenduski (2016), Timescales for detection of trends in the ocean carbon sink, *Nature*, *530*(7591), 469–472.

McKinley, G. A., A. R. Fay, N. S. Lovenduski, and D. J. Pilcher (2017), Natural variability and anthropogenic trends in the ocean carbon sink, *Annu. Rev. Mar. Sci.*, *9*(1), 125–150, doi:10.1146/annurev-marine-010816-060529.

Mills, M. J., O. B. Toon, J. Lee-Taylor, and A. Robock (2014), Multidecadal global cooling and unprecedented ozone loss following a regional nuclear conflict, *Earth's Future*, *2*(4), 161–176, doi:10.1002/2013EF000205.

Moore, J. K., and O. Braucher (2008), Sedimentary and mineral dust sources of dissolved iron to the world ocean, *Biogeosciences*, *5*(3), 631–656.

Moore, J. K., S. C. Doney, and K. Lindsay (2004), Upper ocean ecosystem dynamics and iron cycling in a global three-dimensional model, *Global Biogeochem. Cycles*, *18*(4), GB4028, doi:10.1029/2004GB002220.

Moore, J. K., K. Lindsay, S. C. Doney, M. C. Long, and K. Misumi (2013), Marine ecosystem dynamics and biogeochemical cycling in the Community Earth System Model [CESM1(BGC)]: Comparison of the 1990s with the 2090s under the RCP4.5 and RCP8.5 scenarios, *J. Climate*, *26*(23), 9291–9312, doi:10.1175/JCLI-D-12-00566.1.

Negrete-García, G., N. S. Lovenduski, C. Hauri, K. M. Krumhardt, and S. K. Lauvset (2019), Sudden emergence of a shallow aragonite saturation horizon in the Southern Ocean, *Nature Clim. Change*, *9*(4), 313–317, doi:10.1038/s41558-019-0418-8.

Özdoğan, M., A. Robock, and C. J. Kucharik (2013), Impacts of a nuclear war in South Asia on soybean and maize production in the Midwest United States, *Clim. Chang.*, *116*(2), 373–387, doi:10.1007/s10584-012-0518-1.

Pausata, F. S. R., J. Lindvall, A. M. L. Ekman, and G. Svensson (2016), Climate effects of a hypothetical regional nuclear war: Sensitivity to emission duration and particle composition, *Earth's Future*, *4*(11), 498–511, doi:10.1002/2016EF000415.

Pörtner, H.-O., D. M. Karl, P. W. Boyd, W. W. L. Cheung, S. E. Lluch-Cota, Y. Nojiri, D. N. Schmidt, and P. O. Zavialov (2014), Ocean systems, in *Climate Change 2014: Impacts, Adaptation, and Vulnerability. Part A: Global and Sectoral Aspects. Contribution of Working Group II to the Fifth Assessment Report of the Intergovernmental Panel on Climate Change*, edited by C. B. Field, V. R. Barros, D. J. Dokken, K. J. Mach, M. D. Mastrandrea, T. E. Bilir, M. Chatterjee, K. L. Ebi, Y. O. Estrada, R. C. Genova, B. Girma, E. S. Kissel, A. N. Levy, S. MacCracken, P. R. Mastrandrea, and L. L. White, pp. 411–484, Cambridge University Press, United Kingdom and New York, NY, USA.

Ricke, K. L., J. C. Orr, K. Schneider, and K. Caldeira (2013), Risks to coral reefs from ocean carbonate chemistry changes in recent earth system model projections, *Environ. Res. Lett.*, *8*(3), 034,003.

Robock, A., L. Oman, G. L. Stenchikov, O. B. Toon, C. Bardeen, and R. P. Turco (2007), Climatic consequences of regional nuclear conflicts, *Atmos. Chem. Phys.*, *7*(8), 2003–2012, doi:10.5194/acp-7-2003-2007.

Sarmiento, J. L., and N. Gruber (2006), *Ocean Biogeochemical Dynamics*, Princeton University Press, Princeton, NJ, USA.

Toon, O. B., C. G. Bardeen, A. Robock, L. Xia, H. Kristensen, M. McKinzie, R. J. Peterson, C. S. Harrison, N. S. Lovenduski, and R. P. Turco (2019), Rapidly expanding nuclear arsenals in Pakistan and India portend regional and global catastrophe, *Sci. Adv.*, *5*(10), eaay5478, doi:10.1126/sciadv.aay5478.

Turco, R. P., O. B. Toon, T. P. Ackerman, J. B. Pollack, and C. Sagan (1983), Nuclear winter: Global consequences of multple nuclear explosions, *Science*, *222*(4630), 1283, doi:10.1126/science.222.4630.1283.

van Heuven, S., D. Pierrot, J. W. B. Rae, E. Lewis, and D. W. R. Wallace (2011), MATLAB Program developed for CO_2 system calculations, *Tech. Rep. ORNL/CDIAC-105b*, Carbon Dioxide Information Analysis Center, Oak Ridge National Laboratory, US Department of Energy, Oak Ridge, Tennessee, doi: 10.3334/CDIAC/otg.CO2SYS_MATLAB_v1.1.

Waldbusser, G. G., B. Hales, C. J. Langdon, B. A. Haley, P. Schrader, E. L. Brunner, M. W. Gray, C. A. Miller, and I. Gimenez (2014), Saturation-state sensitivity of marine bivalve larvae to ocean acidification, *Nature Clim. Change*, *5*, 273 EP –.

Xia, L., and A. Robock (2013), Impacts of a nuclear war in South Asia on rice production in Mainland China, *Clim. Chang.*, *116*(2), 357–372, doi:10.1007/s10584-012-0475-8.
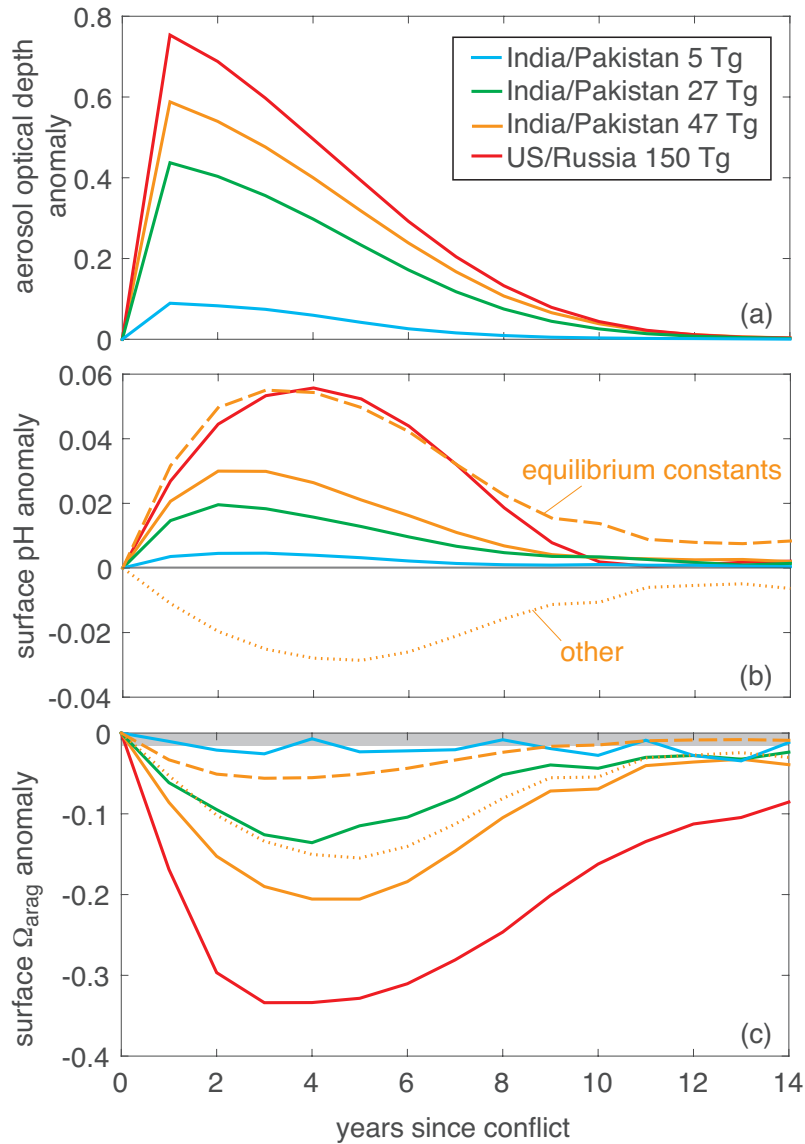
Figure 1. Temporal evolution of the annual mean, globally averaged anomaly in (a) aerosol optical depth, (b) surface ocean pH, and (c) surface ocean Ω_{arag} for the first 14 years following each conflict. In each case, the anomaly represents the difference between the conflict simulation and the ensemble mean of the three control simulations. Gray shading in panels (b) and (c) shows one standard deviation of the annual-mean anomalies in pH and Ω_{arag}, respectively, from the control ensemble means. Dashed orange lines in panels (b) and (c) represent the anomalies in pH and Ω_{arag} driven by changes in the carbonate system equilibrium constants for the India/Pakistan 47 Tg simulation, and the dotted lines represent all other drivers of the anomalies.
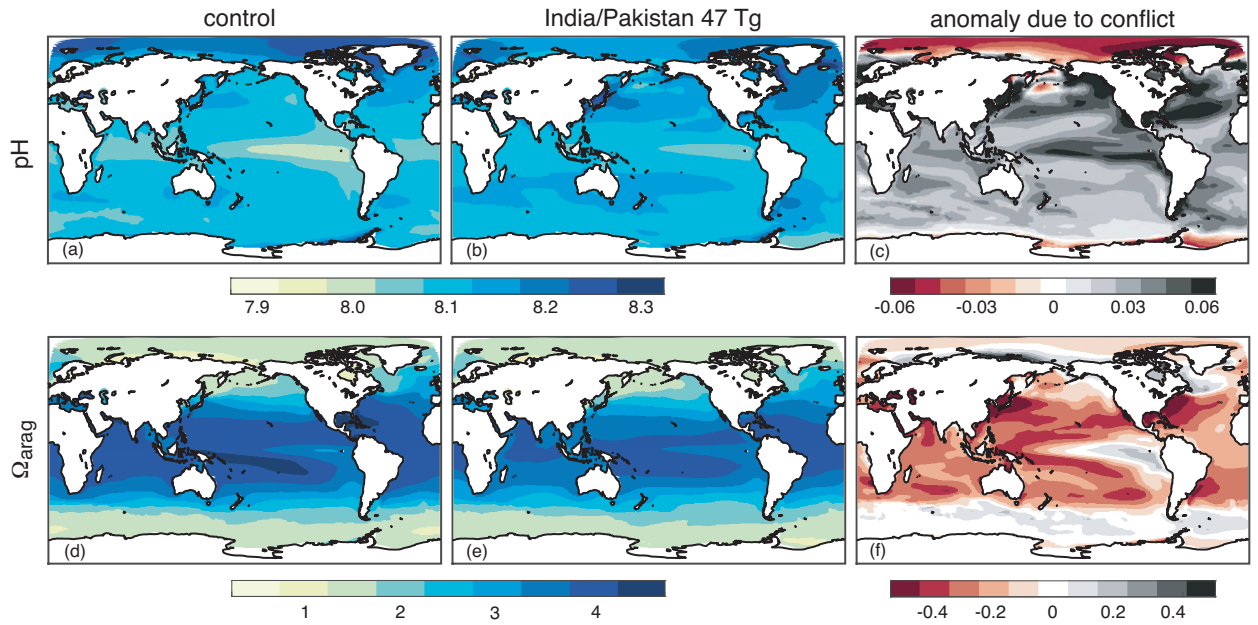
Figure 2. Annual mean surface ocean (top row) pH and (bottom row) Ω_{arag} averaged over years 2-5 post-conflict of the (first column) control simulation ensemble mean, and (second column) Indian/Pakistan 47 Tg simulation. (third column) Anomaly due to conflict, represented as the difference between the 47 Tg simulation and the control ensemble mean in years 2-5 post-conflict.
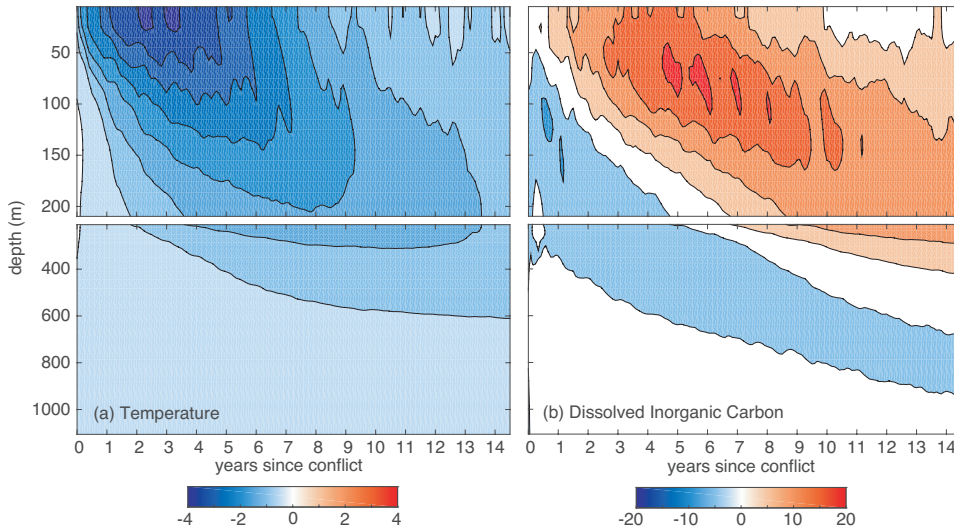
Figure 3. Temporal evolution of the globally averaged anomalies in (a) temperature ($^{\circ}$C) and (b) salinity normalized dissolved inorganic carbon (mmol m^{-3}) from the surface to 1000 m for the first 14 years following the India/Pakistan 47 Tg conflict. Anomalies defined as in Figure 1.